Dalton Transactions

ROYAL SOCIETY OF CHEMISTRY

PAPER

View Article Online
View Journal | View Issue

Cite this: *Dalton Trans.*, 2024, **53**, 15913

Encapsulation of the vanadium substituted Keggin polyoxometalates $[\alpha\text{-}PVW_{11}O_{40}]^{4-}$ and $[\alpha\text{-}PV_2W_{10}O_{40}]^{5-}$ in HKUST-1†

José C. Orozco,[a] Damola T. Shuaib,[a] LaSalle Swenson,[a] Ying-Pin Chen,[b] Yu-Sheng Chen[b] and M. Ishaque Khan *[a]

Received 11th June 2024,
Accepted 6th September 2024

DOI: 10.1039/d4dt01705f

rsc.li/dalton

Two POM@MOF hybrid materials composed of a copper-based metal–organic framework (MOF) $[Cu_3(C_9H_3O_6)_2(H_2O)_3]_n$ (HKUST-1) encapsulating vanadium-substituted Keggin polyoxometalates (POM), $[\alpha\text{-}PVW_{11}O_{40}]^{4-}$ (**PVW_{11}**) and $[\alpha\text{-}PV_2W_{10}O_{40}]^{5-}$ (**PV_2W_{10}**), were prepared and characterized. PVW_{11}@HKUST-1 and PV_2W_{10}@HKUST-1 were synthesized hydrothermally by self-assembly of HKUST-1 in the presence of the preformed POMs, $[\alpha\text{-}PVW_{11}O_{40}]^{4-}$ and $[\alpha\text{-}PV_2W_{10}O_{40}]^{5-}$, respectively. The two POM@MOF composites were characterized by X-ray diffraction, TGA, BET surface area analysis and FT-IR and Raman spectroscopy. The electronic structure of the POM@MOF materials and their respective constituents is surveyed using solid state UV-vis reflectance spectroscopy. The UV-vis spectra order the oxidizing strength of the POM constituents ($[\alpha\text{-}PV_2W_{10}O_{40}]^{5-}$ > $[\alpha\text{-}PVW_{11}O_{40}]^{4-}$) and reveal the distinct electronic structure of the POM@MOF materials obtained by synthetic encapsulation of mono- and di-vanadium substituted Keggin polyoxotungstates in HKUST-1.

1. Introduction

Polyoxometalates (POMs) are transition metal–oxide clusters composed of (mainly) V, Mo, or W cations bridged by oxide ions.[1–3] POMs contain (electro)chemically addressable redox centers and absorb in the near-UV.[3–5] As active molecular species, POMs have been applied in a variety of technical areas, including catalysis,[6,7] photocatalysis,[4,8] biomedicine,[9] magnetism[10] and energy storage and conversion.[11–18] Technical applications often require or are enhanced by POM heterogenation. The non-covalent immobilization of POMs in the pores of metal–organic framework (MOF) materials (designated POM@MOF) has received much recent attention as a POM heterogenation strategy.[19,20] This approach supports the active POM constituent in a nanoporous, high surface area, crystalline functional matrix. Although host–guest interactions are always present, as a conceptual starting point, the POM active center may be considered chemically isolated from the MOF host, making the POM@MOF motif compatible with a materials design approach based on the physical and chemical properties of the separate MOF and POM constituents. An early example combines the pore structure of a Cu/benzene tricarboxylate-based MOF with the catalytic activity of a POM $[H_3(PW_{12}O_{40})]$ to adsorb and subsequently decompose dimethyl methylphosphonate (a nerve gas mimic) by acid catalyzed hydrolysis.[21] Another early example demonstrated catalytic size selectivity for the acid hydrolysis of a series of esters.[22] (Photo)catalytic,[20,22,23,28] (photo)electrocatalytic,[29,30] and energy storage and conversion[23,31] applications are lively current research areas. Synergistic effects of activity and stability are also observed.[19–27]

The Keggin structure polyoxoanion, $(XM_{12}O_{40})^{-\delta}$ (M = Mo^{VI} or W^{VI}) (Fig. 1a and b), has been extensively investigated in homogeneous and heterogeneous (photo)oxidative catalysis[6,32,33] and has received much recent attention as a supported (photo)electrocatalytic center, including POM@MOF examples.[23,29] Both the Mo and W analogues can support V^V substitution to form vanadium-substituted molybdates and tungstates $[(XV_nM_{12-n}O_{40})^{-\delta}$ (M = Mo, W; n = 1, 2, 3)]. The vanadium addenda have greater oxidizing strength than either the Mo or W addenda.[32,34,35] Vanadium-substituted POM are active in a variety of oxidation processes[23,36–53] and have also been evaluated as electrocatalysts.[54] POM@MOF materials containing Keggin structure POMs have been reported,[25–27] including vanadium-substituted molybdates

[a]*Department of Chemistry, Illinois Institute of Technology, Chicago, IL 60616, USA. E-mail: khan@iit.edu*

[b]*ChemMatCARS, The University of Chicago, Lemont, IL 60439, USA*

†Electronic supplementary information (ESI) available: Representations of **2**; crystallographic data tables for **1** and **2**; hydronium ion position discussion; IR spectra of **2**, TGA, BET surface area. CCDC 2249036 and 2249037. For ESI and crystallographic data in CIF or other electronic format see DOI: https://doi.org/10.1039/d4dt01705f

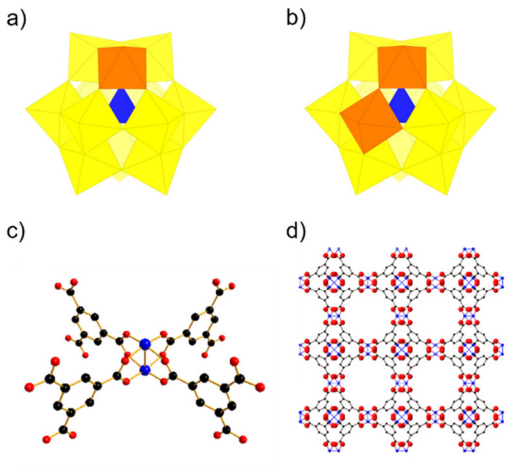

Fig. 1 Polyhedral representations of the Keggin structure polyoxoanions (a) $[\alpha\text{-}PVW_{11}O_{40}]^{4-}$ and (b) $[\alpha\text{-}PV_2W_{10}O_{40}]^{5-}$. Tungsten-centered octahedra are represented in yellow and the orange octahedra depict vanadium substitution. The tetrahedral coordination of the centrally located phosphorous heteroatom is shown in blue. (c) Ball-and-stick representation of the dicopper(II) tetracarboxylate building block of the MOF HKUST-1. (d) HKUST-1 framework viewed along the [100] direction. The $d \sim 1$ nm channels intersect to form pores ($d \sim 1.1$ nm) connected by a 3D network.[54] Color code: V orange; W yellow; P indigo; Cu blue; C black; and O red.

$(XV_nMo_{12-n}O_{40})^{-\delta}$.[20,23,24,55] The MOF HKUST-1 (also known as MOF-199) is composed of dicopper(II) metal centers joined by benzene-1,3,5-tricarboxylate linkers (Fig. 1c and d). HKUST-1 contains a 3D porous (9 × 9 Å) network; and cavities ($d \sim 1.1$ nm) are present at the intersection of pores.[56,57] HKUST-1 is a redox-active material,[54,58] contains a near-UV (*ca.* 375 nm) ligand-to-metal charge-transfer band, and has been investigated as the active component of faradaic supercapacitors.[58] The HKUST structure has been synthesized using a variety of transition metals (*e.g.*, Mo^{2+}, Fe^{2+}, Cr^{2+}, Ni^{2+}, Zn^{2+}),[59–63] and mixed metal analogues have also been reported. A number of POM@HKUST-1 examples have been reported,[23,25–27] including, concurrent with the preparation of this manuscript, a POM@HKUST-1 incorporating the vanadium mono-substituted phosphotungstate Keggin anion, $[\alpha\text{-}PV_1W_{11}O_{40}]^{5-}$ (**PVW_{11}**) (designated PVW_{11}@HKUST-1 (**1**) herein).[24] In this work, we report the synthesis of **1** using tetramethyl ammonium chloride (**TMACl**) in place of tetramethyl ammonium hydroxide (**TMAOH**), which we also use to encapsulate the vanadium di-substituted phosphotungstate Keggin anion, $[\alpha\text{-}PV_2W_{10}O_{40}]^{5-}$ (**PV_2W_{10}**), in HKUST-1 to form PV_2W_{10}@HKUST-1 (**2**). POM@MOF materials containing vanadium-substituted Keggin structure molybdates and tungstates $(XV_nM_{12-n}O_{40})^{-\delta}$ (M = Mo, W) have demonstrated catalytic oxidative activity on a variety of substrates, including 2-chloroethyl ethyl sulfide,[64] cyclohexene,[65] thiols,[66] alcohols,[67] and ascorbic acid (electrocatalytic).[68] Therefore oxidative catalysis is a prospective application of **1** and **2**. We also use UV-vis reflectance spectroscopy to show that the electronic structures of **1** and **2** appear composite of their constituents.

2. Experimental

Infrared spectra (1% KBr pellet) were recorded using a Thermo Nicolet NEXUS 470 spectrometer and evaluated using OMNIC and Origin 9.1 software. Thermogravimetric analysis was performed on a Mettler Toledo SDTA/TGA 851e thermogravimetric analyzer (TGA) in an inert atmosphere (Ar, 50 mL min^{-1}) with a heating rate of 5 °C min^{-1} in the temperature range of 25–800 °C. The resulting TGA curves were processed using Mettler Toledo's STARe v10.0 software and Origin 9.1 software. Raman spectra were recorded using a Renishaw inVia™ confocal Raman Microscope (solid sample, λ_e = 514 nm) equipped with a CCD camera detector. The spectra were processed using Renishaw's Wire3.4 software and Origin 9.1 software. Elemental analyses were performed by the University of Illinois (Urbana-Champaign) Microanalysis Laboratory and Robertson Microlit Laboratories (Ledgewood, NJ). Sample degassing, surface area measurements, and N_2 adsorption/desorption isotherms were measured using a Quantachrome Instruments NOVA 2200e surface area analyzer. Reflectance spectra of powdered samples of **1** and **2** were obtained using an Ocean Optics HR4000 spectrometer controlled by Ocean Optics Spectra Suite Spectrometer Operating Software and an in-house constructed dark chamber fitted with a UV–Vis–NIR light source (Mikropack, DH-2000-BAL). Reflectance was measured against a Labsphere certified reflectance standard (USRS-99-010) and is reported as a pseudo-absorbance obtained by subtracting the reflectance (R) from unity. Single crystal X-ray data were collected using synchrotron radiation (λ = 0.41328 Å) at Advanced Photon Source (APS), Argonne National Laboratory (ANL). Crystals suitable for X-ray diffraction were mounted on a glass fiber and transferred to a Huber three-circle diffractometer equipped with a PILATUS3 X 2M detector. The collected diffraction frames were integrated using SAINT V8.40B and scaled with a multi-scan absorption correction.[69,70] Crystals of compounds **1** and **2** were kept in a nitrogen atmosphere at 100 K during data collection. Using Olex2, the structures were solved with the ShelXT structure solution program[71] with intrinsic phasing method and refined by full-matrix least-squares on F^2 with the ShelXL refinement package.[72] All non-hydrogen atoms were refined anisotropically.[73,74] The crystal data, data collection and refinement parameters are summarized in Table 1. Crystallographic data are available free of charge from the Cambridge Crystallographic Data Centre under CCDC 2249036 and 2249037.†

Synthesis of vanadium-substituted phosphotungstates

All reagents were obtained from commercial sources and used without further purification. We synthesized potassium salts of the vanadium-substituted Keggin anions $[\alpha\text{-}PVW_{11}O_{40}]^{4-}$ **PVW_{11}** and $[\alpha\text{-}PV_2W_{10}O_{40}]^{5-}$ **PV_2W_{10}**. $K_4[\alpha\text{-}PVW_{11}O_{40}]\cdot 2H_2O$ was synthesized by reacting $K_7PW_{11}O_{39}$ with sodium metavanadate according to a reported procedure[75,76] and the purity of the product was confirmed by Fourier transform infrared (FT-IR)

Table 1 X-ray crystal data for compounds **1** and **2**

Compound	**1** (CCDC 2249036)	**2** (CCDC 2249037)
Empirical formula	$C_{80}H_{98}Cu_{12}N_2O_{112}PVW_{11}$	$C_{80}H_{99}Cu_{12}N_2O_{114}PV_2W_{10}$
Formula weight	5746.34	5646.44
Temperature/K	100(2)	100(2)
Crystal system	Cubic	Cubic
Space group	$Fm\bar{3}m$	$Fm\bar{3}m$
a/Å	26.2682(12)	26.2682(12)
b/Å	26.2682(12)	26.2682(12)
c/Å	26.2682(12)	26.2682(12)
α/°	90	90
β/°	90	90
γ/°	90	90
Volume/Å^3	18 126(2)	18 126(2)
Z	4	4
ρ_{calc} g cm^{-3}	2.106	2.069
μ/mm^{-1}	2.037	1.895
F(000)	10 752	10 616
Crystal size/mm^3	0.1 × 0.05 × 0.05	0.1 × 0.05 × 0.05
Radiation, λ (synchrotron)	0.41328	0.41328
2Θ range for data collection/°	1.802 to 27.792	1.802 to 27.792
Completeness to theta	99.9%	99.9%
Index ranges	$-30 \le h \le 30$, $-30 \le k \le 30$, $-30 \le l \le 30$	$-30 \le h \le 30$, $-30 \le k \le 30$, $-30 \le l \le 30$
Reflections collected	99 252	87 447
Independent reflections	812 [R_{int} = 0.1620, R_{sigma} = 0.0299]	812 [R_{int} = 0.1194, R_{sigma} = 0.0312]
Data/restraints/parameters	812/9/73	812/15/77
Goodness-of-fit on F^2	1.098	1.172
Final R indexes [$I \ge 2\sigma(I)$]	R_1 = 0.0486, wR_2 = 0.1416	R_1 = 0.0597, wR_2 = 0.1709
Final R indexes [all data]	R_1 = 0.0601, wR_2 = 0.1594	R_1 = 0.0691, wR_2 = 0.1911
Largest diff. peak/hole/e Å^{-3}	1.585/−1.612	1.189/−1.651

$R_1 = \sum|F_o| - |F_c|/\sum|F_o|$. w$R_2 = [\sum[w(F_o^2 - F_c^2)^2]/\sum[w(F_o^2)^2]]^{1/2}$.

spectroscopy. 1,2-$K_5[\alpha\text{-}PV_2W_{10}O_{40}]$ was prepared using a reported procedure.[77]

Synthesis of POM@MOF materials

Synthesis of PVW_{11}@HKUST-1 (1). $K_4[\alpha\text{-}PVW_{11}O_{40}]\cdot 2H_2O$ (0.1 mmol, 294 mg), $Cu(NO_3)_2\cdot 3H_2O$ (2.5 mmol, 604 mg), 1,3,5-benzenetricarboxylic acid ($C_6H_3(CO_2H)_3$, 2.0 mmol, 420 mg), and $(CH_3)_4NCl$ (1.0 mmol, 110 mg) were combined in a Teflon lined Parr reaction vessel. 10 mL of deionized water was added to the vessel and the vessel was transferred to a temperature programmed furnace and heated at 2 °C min^{-1} to 200 °C, held for 15 h at 200 °C, cooled at a programmed rate of 0.1 °C min^{-1} to 100 °C, held for 4 h at 100 °C, and then allowed to cool to room temperature. The resulting product was washed with boiling water several times until the filtrate became clear, washed with *N*,*N*-dimethylformamide (DMF) several times to remove light blue amorphous impurities, and finally washed with acetone three times. The bluish-green octahedra-shaped crystals were separated mechanically from tiny blue needle block crystals of $[Cu_2(C_9O_6H_3)(OH)(H_2O)]_n\cdot 2nH_2O$ – which competes with the formation of HKUST-1.[78,79] The final product was stored in a desiccator at room temperature. The pure bluish-green crystalline solid was used for further characterization. Yield *ca.* 150 mg (26% based on $K_4[\alpha\text{-}PVW_{11}O_{40}]$). Elemental analysis calcd (%) for $C_{80}H_{178}Cu_{12}N_2O_{152}PVW_{11}$ (5746.34): C 14.86, H 2.77, N 0.43, Cu 11.79, V 0.79; found C 15.72, H 2.01, N 0.8, Cu 12.1, V 0.82. PV_2W_{10}@HKUST-1 (**2**) was prepared by the above procedure using preformed 1,2-$K_5[\alpha\text{-}PV_2W_{10}O_{40}]\cdot 3H_2O$ (0.1 mmol, 286 mg) in place of $K_4[\alpha\text{-}PVW_{11}O_{40}]\cdot 2H_2O$. Green octahedral crystals were obtained. Yield *ca.* 150 mg, (27% based on 1,2-$K_5[\alpha\text{-}PV_2W_{10}O_{40}]$). Elemental analysis calcd (%) for $C_{80}H_{179}Cu_{12}N_2O_{154}PV_2W_{10}$ (5646.44): C 15.09, H 2.83, N 0.44, Cu 11.98, V 1.6, found C 15.93, H 2.54, N 0.76, Cu 13.44, V 0.9.

3. Results and discussion

The Keggin structure anion $(XM_{12}O_{40})^{-\sigma}$ contains twelve octahedrally-coordinated addenda atoms. Its structure may be considered as four M_3O_{13} groups linked through corner-sharing (Fig. 1a and b). Each M-centered octahedra within an M_3O_{13} group shares an edge with each of the remaining two octahedra. A heteroatom (X), located at the center of the structure is tetrahedrally coordinated to a shared μ_3-oxygen of each M_3O_{13} group. The synthetic procedure forming **PV_2W_{10}** locates the substituted vanadium cations as corner-sharing neighbors in separate M_3O_{13} groups (Fig. 1b). Watras and Teplyakov benchmarked this arrangement using FTIR spectroscopy,[80] and we apply that procedure here, *vide infra*. One approach to obtain POM@MOF materials, sometimes referred to as *synthetic encapsulation*, is to synthesize the MOF in the presence of pre-formed POM with the intention of encapsulating the POM as the MOF forms. A number of Keggin@HKUST-1 materials, where the Keggin anion is encapsulated in the large pores ($d \sim 1.1$ nm) of HKUST-1, have been obtained by this approach.[20,23] Here we obtain

PVW_{11}@HKUST-1 and PV_2W_{10}@HKUST-1 by synthetic encapsulation using **TMACl** in place of **TMAOH**, the usual reagent associated with Keggin@MOF structures by synthetic encapsulation. While we could obtain PVW_{11}@HKUST-1 using **TMAOH**, we could not obtain PV_2W_{10}@HKUST-1. We found that both POM@MOF structures could be obtained using **TMACl**.

Structure

Single crystal X-ray diffraction analysis of **1** and **2** (crystallographic data is shown in Table 1) shows that respective Keggin anions are encapsulated in the large pores of HKUST-1. Structural features of **1** are shown in Fig. 2 (see ESI† for additional crystallographic data). Positional disorder of monovanadium and di-vanadium substitution was revealed, which is a common feature of α-Keggin type POMs.[25] The tetramethylammonium $C_4H_{12}N^+$ (TMA) and H_3O^+ provide charge balance to the Keggin anion species $[\alpha\text{-}PVW_{11}O_{40}]^{4-}$ and $[\alpha\text{-}PV_2W_{10}O_{40}]^{5-}$ in compounds **1** and **2**. The tetramethylammonium (**TMA**) cations, $C_4H_{13}N^+$ (N1S–C1S), were assigned to have full occupancy in the composites **1** and **2**, accounting for the two units of positive charge. This assignment is consistent with a previous report of the presence of **TMA** cations for charge compensation in POM@MOFs composed of HKUST-1 containing POM ($[SiMo_{12}O_{40}]^{4-}$, $[PW_{12}O_{40}]^{3-}$, and $[PMo_6W_6O_{40}]^{4-}$).[27] The remaining charge balance is provided by hydronium ions, 2 and 3 units, respectively, in **1** and **2**. The possible positions to assign H_3O^+ were on O1w, O2w or O3w (Fig. 2a and S1;† see ESI† for further discussion).

TGA and BET surface area

Thermogravimetric analysis shows that **1** and **2** are stable to *ca.* 250 °C, in line with the reported 240 °C stability of HKUST-1[56] (Fig. S6†). The Brunauer–Emmett–Teller (BET) surface area of HKUST-1 (674 $m^2\ g^{-1}$, Fig. S7†) is near the first reported value (692 $m^2\ g^{-1}$).[56] The BET surface areas of **1** (145 $m^2\ g^{-1}$) and **2** (261 $m^2\ g^{-1}$) are consistent with the reduction of HKUST-1 surface area expected upon POM encapsulation.

IR spectroscopy

The FTIR and Raman spectra of **1** and **2** contain bands consistent with POM@MOF formation. In FTIR spectra, the $\mathbf{PVW_{11}}$ and $\mathbf{PV_2W_{10}}$ species can be identified by characteristic features in the *ca.* 1025–1125 cm^{-1} region, where $\mathbf{PVW_{11}}$ and $\mathbf{PV_2W_{10}}$ exhibit two and three bands, respectively.[80] These identifying bands are present in the $\mathbf{PVW_{11}}$ and $\mathbf{PV_2W_{10}}$ spectra and the respective spectra of **1** and **2** (Fig. 3 and S4†). The strong $W{=}O_t$ band appearing in $\mathbf{PVW_{11}}$ and $\mathbf{PV_2W_{10}}$ (980 and 962 cm^{-1}) appears blue shifted in the spectra of **1** and **2** (986 and 974 cm^{-1}). A band associated with edge-sharing oxygen ($W{-}O_c{-}W$) appearing in $\mathbf{PVW_{11}}$ and $\mathbf{PV_2W_{10}}$ (794 and 789 cm^{-1}), splits into two distinct bands in **1** (824 and 797 cm^{-1}) and **2** (820 and 796 cm^{-1}). The Raman spectrum of HKUST-1 (Fig. 4 and S5†) contains a strong band around 1010 cm^{-1} associated with $\nu(C{=}C)$ modes of benzene; and strong bands associated with out-of-plane ring (C–H) bending vibrations (825 cm^{-1}) and out-of-plane ring bending (740 cm^{-1}); bands below 600 cm^{-1} are associated with the Cu(II) species.[81] In the Raman spectra of $\mathbf{PVW_{11}}$ and $\mathbf{PV_2W_{10}}$ (Fig. S5†) strong bands associated with the symmetric and asymmetric stretch of the terminal oxygen atom ($W{=}O_t$) appear around 1000 cm^{-1}; weaker bands associated with bridging oxygen atoms are present below 950 cm^{-1}. The Raman spectra of **1** (Fig. 4) and **2** (Fig. S5†) appear composite of their

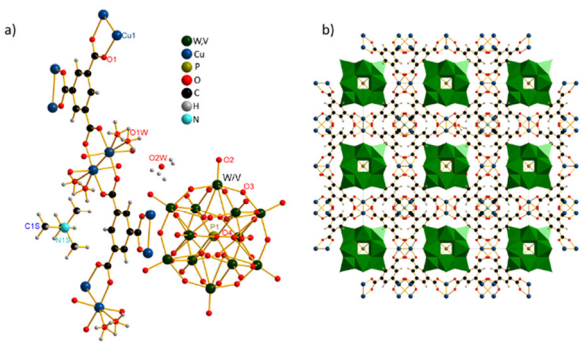

Fig. 2 (a) A structural fragment of PVW_{11}@HKUST-1. The vanadium and tungsten atoms occupy the same crystallographic site in each $[PVW_{11}O_{40}]^{4-}$ anion, with occupancies of 0.08 and 0.92, respectively. (b) Structure of PVW_{11}@HKUST-1 viewed along the [100] direction. Positional disorder of encapsulated Keggin anions is not depicted. Selected bond lengths [Å] and angles [°]: **1**; W1–O3 1.890(4), W1–O2 1.681(13), W1–O4 2.478(14), Cu1–Cu1[4] 2.639(4), Cu1–O1 1.948(6), Cu1–O1 W 2.187(15), P1–O4 1.52(3); O3–W1–O3 86.8(5), O3–W1–O3 155.7 (8), O3–W1–O3 88.2(6), O3–W1–O4 92.8(5), O2–W1–O3 102.1(4), O2–W1–O4 159.3(5), O1–Cu1–Cu1 84.61(19), O1–Cu1–O1 90.2(4), O1–Cu1–O11 87.4(4), O1–Cu1–O11 103.2(4), O4–P1–O4 109.471(2). [4]1/2 – *X*, 1 – *Y*, 1/2 – *Z* (see ESI†).

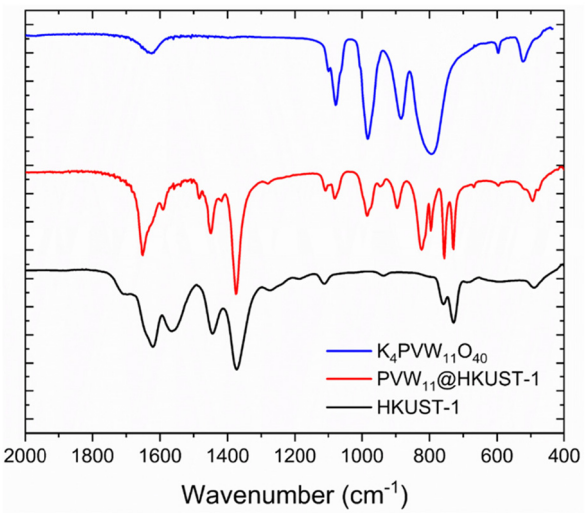

Fig. 3 FTIR spectra of **1** and its constituents HKUST-1 and the monovanadium substituted Keggin POM $K_4[\alpha\text{-}PVW_{11}O_{40}]$ in the 2000–400 cm^{-1} range. Prominent bands in the FTIR spectrum of **1** (cm^{-1}): 1651 (s), 1591 (m), 1483 (m), 1448 (s), 1417 (m, sh), 1375 (s), 1281 (w), 1109 (w), 1080 (w), 986 (w), 947 (w), 897 (w), 824 (s), 797 (m), 756 (s), 729 (s), 669 (w), 596 (w), 496 (w), 478 (w, sh).

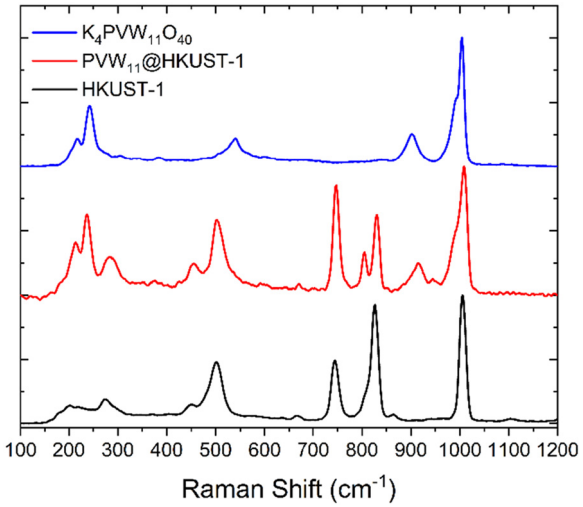

Fig. 4 Raman spectra of **1** and its constituents HKUST-1 and the mono-vanadium substituted Keggin POM $K_4[\alpha\text{-}PVW_{11}O_{40}]$ in the 100–1200 cm^{-1} range.

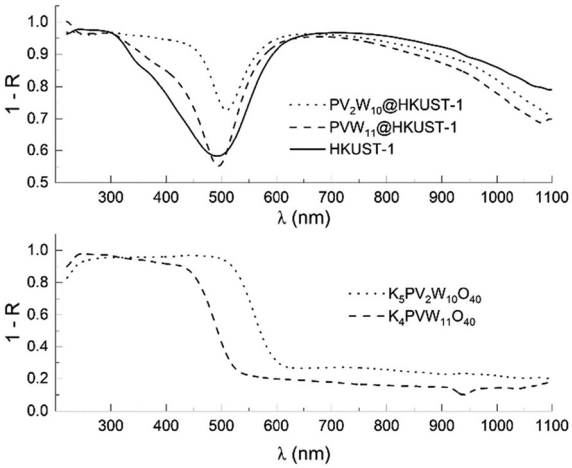

Fig. 5 UV–Vis–NIR (220–1100 nm) reflectance spectra of **1**, **2** and HKUST-1 (top panel) and $K_4PVW_{11}O_{40}$ and $K_5PV_2W_{10}O_{40}$ (bottom panel). A reflectance fraction (R) was obtained by comparison to a reflectance standard and pseudo absorption spectra were derived by subtracting R from unity (plotted).

separate POM and MOF constituents with the exception of a weak feature around 950 cm^{-1} that cannot be directly attributed to either constituent. The band appearing around 900 cm^{-1} in the spectra of **PVW_{11}** and **PV_2W_{10}** is associated with bridging oxygen atoms and exhibits a distinct blue-shift in the spectra of **1** and **2**.[82,83]

UV-vis reflectance spectroscopy

Each M-centered coordination sphere of the Keggin structure anion contains a terminal oxygen atom. Metal–oxygen ($M\text{–}O_t$) orbital overlap supports ligand-to-metal charge transfer (**LMCT**) from occupied orbitals formally delocalized on the peripheral oxo ligands (**HOMO**) to unoccupied d-metal orbitals (**LUMO**), which are also delocalized at room temperature.[34] Keggin structure anions typically exhibit reversible redox activity and absorption initiating in the UV (Mo^{VI} and W^{VI}). Vanadium substitution has been shown to modify the relative energy of the **LUMO** (DFT)[34] and it is well-established that the ease of reduction of POM addenda follows the order $V^{IV} > Mo^{VI} > W^{VI}$.[3,5,29] Solid-state UV-vis reflectance spectroscopy is a convenient method to survey electronic structure while minimizing solvent effects. Reflectance spectra covering the UV, visible, and a portion of the near-IR range of $K_4PVW_{11}O_{40}$, $K_5PV_2W_{10}O_{40}$, HKUST-1, **1** and **2** are plotted as pseudo-absorbances ($1 - R$) in Fig. 5. We can attribute the initial portion of the broad high energy band observed in the spectra of $K_4PVW_{11}O_{40}$ and $K_5PV_2W_{10}O_{40}$ to **LMCT** originating at the vanadium-substituted octahedra. Both bands initiate in the visible range ($K_4PVW_{11}O_{40}$ ~ 525 nm; $K_5PV_2W_{10}O_{40}$ ~ 600 nm) and remain well-separated until each plateau. **LMCT** bands correlate to reduction potentials, implying that the $K_5PV_2W_{10}O_{40}$ species, which contains corner-shared vanadium-centered octahedra, is easier to reduce than $K_4PVW_{11}O_{40}$, that is, that it is a stronger oxidizing agent. The HKUST-1 spectrum contains UV and visible bands originating in d–d (vis), π–π* (initial UV), and LMCT (shoulder at 375 nm) transitions.[81,84] The **POM@MOF** spectra appear roughly additive of their respective constituents by comparison. This is apparent in the broad feature initiating in the IR and in the onset regions of the high energy bands associated with the **POM** constituents, which remain well-separated in **1** and **2**. Thus the UV-vis spectra are consistent with the composite nature of the POM@MOF materials. The retention of the high energy band offsets of the constituents $K_4PVW_{11}O_{40}$ and $K_5PV_2W_{10}O_{40}$ in the POM@MOF materials **1** and **2** supports the materials design potential of the POM@MOF motif, and prospective applications in oxidative catalytic applications, including electro- and photo-oxidative processes.

4. Conclusions

We have demonstrated the synthetic encapsulation of the mono-and di-vanadium substituted Keggin structure POMs $[\alpha\text{-}PVW_{11}O_{40}]^{4-}$ and $[\alpha\text{-}PV_2W_{10}O_{40}]^{5-}$ in the MOF HKUST-1 to form the POM@MOF materials PVW_{11}@HKUST-1 and PV_2W_{10}@HKUST-1, respectively. The hydrothermal synthetic encapsulation procedure uses tetramethylammonium chloride. An electronic structure survey of the POM@MOF materials and their respective constituents using UV-vis reflectance spectroscopy shows that the POM@MOF composite materials have distinct electronic structures that reflect the oxidizing strength of their respective POM constituents ($[\alpha\text{-}PV_2W_{10}O_{40}]^{5-} > [\alpha\text{-}PVW_{11}O_{40}]^{4-}$).

Data availability

The data supporting this article have been included as part of the ESI.†

Crystallographic data for the compounds **1–2** has been deposited at the CCDC under 2249036 (compound **1**) and 2249037 (compound **2**).†

Conflicts of interest

There are no conflicts to declare.

Acknowledgements

Single crystal X-ray diffraction data were collected using synchrotron radiation at NSF's ChemMatCARS Sector 15 at the Advanced Photon source (APS), Argonne National Laboratory (ANL) which is supported by the Divisions of Chemistry (CHE) and Materials Research (DMR), National Science Foundation, under grant number NSF/CHE-1834750. Use of APS, an Office of Science User Facility operated for the U.S. Department of Energy (DOE) Office of Science by ANL, was supported by the U.S. DOE under Contract No. DE-AC02-06CH11357.

References

1 Special thematic issue on polyoxometalates, C. L. Hill (Guest Ed.), *Chem. Rev.*, 1998, **98**, 1–390.
2 Special thematic issue, Polyoxometalate Cluster Science, Leroy Cronin and Achim Müller (Guest Eds.), *Chem. Soc. Rev.*, 2012, **41**, 7333–7646.
3 M. T. Pope, *Heteropoly and Isopoly Oxometalates*, Springer, Verlag, West Berlin, 1983.
4 E. Papaconstantinou and A. Hiskia, in *Polyoxometalate Molecular Science*, ed. J. J. Borrás-Almenar, E. Coronado, A. Müller and M. Pope, Springer, Netherlands, 2003, pp. 381–416.
5 T. Ueda, *ChemElectroChem*, 2018, **5**, 823–838.
6 I. V. Kozhevnikov, *Catalysis by Polyoxometalates: Catalysts for Fine Chemical Synthesis 2*, John Wiley & Sons, West Sussex, England, 2002.
7 J. B. Moffat, *Metal-Oxygen Clusters: The Surface and Catalytic Properties of Heteropoly Oxometalates*, Kluwer Academic Publishers., New York, 2001.
8 G. Marci, E. I. Garcia-Lopez and L. Palmisano, *Eur. J. Inorg. Chem.*, 2014, **2014**, 21–35.
9 M. B. Colovic, M. Lackovic, J. Lalatovic, A. S. Mougharbel, U. Kortz and D. Z. Krsti, *Curr. Med. Chem.*, 2020, **27**, 362–379.
10 J. M. Clemente-Juan, E. Coronado and A. Gaita-Arino, *Chem. Soc. Rev.*, 2012, **41**, 7464–7478.
11 Y. Benseghir, A. Sole-Daura, P. Mialane, J. Marrot, L. Dalecky, S. Bechu, M. Fregnaux, M. Gomez-Mingot, M. Fontecave, C. Mellot-Draznieks and A. Dolbecq, *ACS Catal.*, 2022, **12**, 453–464.
12 L. Chen, W. L. Chen, X. L. Wang, Y. G. Li, Z. M. Su and E. B. Wang, *Chem. Soc. Rev.*, 2019, **48**, 260–284.
13 X. Y. Jia, J. X. Wang, H. B. Hu and Y. F. Song, *Chem. – Eur. J.*, 2020, **26**, 5257–5263.
14 Q. Li, M. Q. Xu, T. Wang, H. J. Wang, J. W. Sun and J. Q. Sha, *Chem. – Eur. J.*, 2022, **28**, e202200207.
15 H. Lv, Y. V. Geletii, C. Zhao, J. W. Vickers, G. Zhu, Z. Luo, J. Song, T. Lian, D. G. Musaev and C. L. Hill, *Chem. Soc. Rev.*, 2012, **41**, 7572–7589.
16 C. L. Peake, A. J. Kibler, G. N. Newton and D. A. Walsh, *ACS Appl. Energy Mater.*, 2021, **4**, 8765–8773.
17 X. Wang, H. Li, J. F. Lin, C. Y. Wang and X. L. Wang, *Inorg. Chem.*, 2021, **60**, 19287–19296.
18 H. Yang, T. Song, L. Liu, A. Devadoss, F. Xia, H. Han, H. Park, W. Sigmund, K. Kwon and U. Paik, *J. Phys. Chem. C*, 2013, **117**, 17376–17381.
19 C. T. Buru and O. K. Farha, *ACS Appl. Mater. Interfaces*, 2020, **12**, 5345–5360.
20 P. Mialane, C. Mellot-Draznieks, P. Gairola, M. Duguet, Y. Benseghir, O. Oms and A. Dolbecq, *Chem. Soc. Rev.*, 2021, **50**, 6152–6220.
21 F.-J. Ma, S.-X. Liu, C.-Y. Sun, D.-D. Liang, G.-J. Ren, F. Wei, Y.-G. Chen and Z.-M. Su, *J. Am. Chem. Soc.*, 2011, **133**, 4178–4181.
22 C.-Y. Sun, S.-X. Liu, D.-D. Liang, K.-Z. Shao, Y.-H. Ren and Z.-M. Su, *J. Am. Chem. Soc.*, 2009, **131**, 1883–1888.
23 M. Samaniyan, M. Mirzaei, R. Khajavian, H. Eshtiagh-Hosseini and C. Streb, *ACS Catal.*, 2019, **9**, 10174–10191.
24 X. Lu, T. Cheng, Y. V. Geletii, J. Bacsa and C. L. Hill, *Catal. Sci. Technol.*, 2023, **13**, 5094–5103.
25 J. Song, Z. Luo, D. K. Britt, H. Furukawa, O. M. Yaghi, K. I. Hardcastle and C. L. Hill, *J. Am. Chem. Soc.*, 2011, **133**, 16839–16846.
26 C.-Y. Sun, S.-X. Liu, D.-D. Liang, K.-Z. Shao, Y.-H. Ren and Z.-M. Su, *J. Am. Chem. Soc.*, 2009, **131**, 1883–1888.
27 L. Yang, H. Naruke and T. Yamase, *Inorg. Chem. Commun.*, 2003, **6**, 1020–1024.
28 J. L. Liu, M. Y. Huang, Z. Y. Hua, Y. Dong, Z. R. Feng, T. D. Sun and C. X. Chen, *ChemistrySelect*, 2022, **7**, e202200546.
29 B. Fabre, C. Falaise and E. Cadot, *ACS Catal.*, 2022, **12**, 12055–12091.
30 C. Freire, D. M. Fernandes, M. Nunes and V. K. Abdelkader, *ChemCatChem*, 2018, **10**, 1703–1730.
31 M. Genovese and K. Lian, *Curr. Opin. Solid State Mater. Sci.*, 2015, **19**, 126–137.
32 C. L. Hill and C. M. Prosser-McCartha, *Coord. Chem. Rev.*, 1995, **143**, 407–455.
33 S. S. Wang and G. Y. Yang, *Chem. Rev.*, 2015, **115**, 4893–4962.
34 J. M. Maestre, X. Lopez, C. Bo, J.-M. Poblet and N. Casañ-Pastor, *J. Am. Chem. Soc.*, 2001, **123**, 3749–3758.
35 M. Sadakane and E. Steckhan, *Chem. Rev.*, 1998, **98**, 219–238.
36 D. M. Fernandes, A. D. S. Barbosa, J. Pires, S. S. Balula, L. Cunha-Silva and C. Freire, *ACS Appl. Mater. Interfaces*, 2013, **5**, 13382–13390.

37 Q. Lan, Z.-M. Zhang, C. Qin, X.-L. Wang, Y.-G. Li, H.-Q. Tan and E.-B. Wang, *Chem. – Eur. J.*, 2016, **22**, 15513–15520.
38 X.-H. Li, Y.-W. Liu, Y. Lu, Z. Zhang, H.-R. Tian, S.-M. Liu and S.-X. Liu, *Chem. Commun.*, 2020, **56**, 1641–1644.
39 Y. Li, Q. Gao, L. Zhang, Y. Zhou, Y. Zhong, Y. Ying, M. Zhang, C. Huang and Y. a. Wang, *Dalton Trans.*, 2018, **47**, 6394–6403.
40 Y. Liu, C. Tang, M. Cheng, M. Chen, S. Chen, L. Lei, Y. Chen, H. Yi, Y. Fu and L. Li, *ACS Catal.*, 2021, **11**, 13374–13396.
41 J. Tong, W. Wang, L. Su, Q. Li, F. Liu, W. Ma, Z. Lei and L. Bo, *Catal. Sci. Technol.*, 2017, **7**, 222–230.
42 Q. Wang and D. Astruc, *Chem. Rev.*, 2020, **120**, 1438–1511.
43 S.-S. Wang and G.-Y. Yang, *Chem. Rev.*, 2015, **115**, 4893–4962.
44 P. Wei, Y. Yang, W. Li and G. Li, *Fuel*, 2020, **274**, 117834.
45 M. Zhang, A. M. Zhang, X.-X. Wang, Q. Huang, X. Zhu, X.-L. Wang, L.-Z. Dong, S.-L. Li and Y.-Q. Lan, *J. Mater. Chem. A*, 2018, **6**, 8735–8741.
46 J. Zhu, M. N. Shen, X. J. Zhao, P. C. Wang and M. Lu, *ChemPlusChem*, 2014, **79**, 872–878.
47 K. Kamata, K. Yonehara, Y. Nakagawa, K. Uehara and N. Mizuno, *Nat. Chem.*, 2010, **2**, 478–483.
48 K. Nomiya, Y. Nemoto, T. Hasegawa and S. Matsuoka, *J. Mol. Catal. A: Chem.*, 2000, **152**, 55–68.
49 K. Nomiya, H. Yanagibayashi, C. Nozaki, K. Kondoh, E. Hiramatsu and Y. Shimizu, *J. Mol. Catal. A: Chem.*, 1996, **114**, 181–190.
50 Y. Nakagawa, K. Kamata, M. Kotani, K. Yamaguchi and N. Mizuno, *Angew. Chem., Int. Ed.*, 2005, **44**, 5136–5141.
51 I. D. Ivanchikova, N. V. Maksimchuk, R. I. Maksimovskaya, G. M. Maksimov and O. A. Kholdeeva, *ACS Catal.*, 2014, **4**, 2706–2713.
52 N. Mizuno and K. Kamata, *Coord. Chem. Rev.*, 2011, **255**, 2358–2370.
53 J. C. Orozco, D. T. Shuaib, C. L. Marshall and M. I. Khan, *React. Kinet., Mech. Catal.*, 2020, **131**, 753–768.
54 D. M. Fernandes and C. Freire, *ChemElectroChem*, 2015, **2**, 269–279.
55 H. Yang, J. Li, L. Wang, W. Dai, Y. Lv and S. Gao, *Catal. Commun.*, 2013, **35**, 101–104.
56 S. S.-Y. Chui, S. M.-F. Lo, J. P. H. Charmant, A. G. Orpen and I. D. Williams, *Science*, 1999, **283**, 1148–1150.
57 A. Vishnyakov, P. I. Ravikovitch, A. V. Neimark, M. Bülow and Q. M. Wang, *Nano Lett.*, 2003, **3**, 713–718.
58 M. Z. Iqbal, M. Shaheen, M. W. Khan, S. Siddique, S. Aftab, S. M. Wabaidur and M. J. Iqbal, *RSC Adv.*, 2023, **13**, 2860–2870.
59 J. I. Feldblyum, M. Liu, D. W. Gidley and A. J. Matzger, *J. Am. Chem. Soc.*, 2011, **133**, 18257–18263.
60 M. Kramer, U. Schwarz and S. Kaskel, *J. Mater. Chem.*, 2006, **16**, 2245–2248.
61 P. Maniam and N. Stock, *Inorg. Chem.*, 2011, **50**, 5085–5097.
62 L. J. Murray, M. Dinca, J. Yano, S. Chavan, S. Bordiga, C. M. Brown and J. R. Long, *J. Am. Chem. Soc.*, 2010, **132**, 7856–7857.
63 Z. Zhang, L. Zhang, L. Wojtas, M. Eddaoudi and M. J. Zaworotko, *J. Am. Chem. Soc.*, 2012, **134**, 928–933.
64 Y. Li, Q. Gao, L. Zhang, Y. Zhou, Y. Zhong, Y. Ying, M. Zhang, C. Huang and Y. Wang, *Dalton Trans.*, 2018, **47**, 6394–6403.
65 J. Tong, W. Wang, L. Su, Q. Li, F. Liu, W. Ma, Z. Lei and L. Bo, *Catal. Sci. Technol.*, 2017, **7**, 222–230.
66 X. Lu, T. Cheng, Y. V. Geletii, J. Bacsa and C. L. Hill, *Catal. Sci. Technol.*, 2023, **13**, 5094–5103.
67 J. Zhu, M. N. Shen, X. J. Zhao, P. C. Wang and M. Lu, *ChemPlusChem*, 2014, **79**, 872–878.
68 D. M. Fernandes, A. D. S. Barbosa, J. Pires, S. S. Balula, L. Cunha-Silva and C. Freire, *ACS Appl. Mater. Interfaces*, 2013, **5**, 13382–13390.
69 *SHELXTL 2018/3*, Bruker-AXS Inc., Madison, 2018.
70 *SADABS 2016/2*, Bruker-AXS Inc., Madison, 2016.
71 G. Sheldrick, *Acta Crystallogr., Sect. A: Found. Adv.*, 2015, **71**, 3–8.
72 G. Sheldrick, *Acta Crystallogr., Sect. A: Found. Crystallogr.*, 2008, **64**, 112–122.
73 O. V. Dolomanov, L. J. Bourhis, R. J. Gildea, J. A. K. Howard and H. Puschmann, *J. Appl. Crystallogr.*, 2009, **42**, 339–341.
74 A. L. Spek, *PLATON/SQUEEZE*, University of Utrecht, 2011.
75 N. Haraguchi, Y. Okaue, T. Isobe and Y. Matsuda, *Inorg. Chem.*, 1994, **33**, 1015–1020.
76 P. J. Domaille, G. Hervéa and A. Téazéa, in *Inorg. Synth*, John Wiley & Sons, Inc., 2007, pp. 96–104.
77 P. J. Domaille, *J. Am. Chem. Soc.*, 1984, **106**, 7677–7687.
78 D. Mustafa, E. Breynaert, S. R. Bajpe, J. A. Martens and C. E. A. Kirschhock, *Chem. Commun.*, 2011, **47**, 8037–8039.
79 M. Schlesinger, S. Schulze, M. Hietschold and M. Mehring, *Microporous Mesoporous Mater.*, 2010, **132**, 121–127.
80 M. J. Watras and A. V. Teplyakov, *J. Phys. Chem. B*, 2005, **109**, 8928–8934.
81 C. Prestipino, L. Regli, J. G. Vitillo, F. Bonino, A. Damin, C. Lamberti, A. Zecchina, P. L. Solari, K. O. Kongshaug and S. Bordiga, *Chem. Mater.*, 2006, **18**, 1337–1346.
82 C. Rocchiccioli-Deltcheff, M. Fournier, R. Franck and R. Thouvenot, *Inorg. Chem.*, 1983, **22**, 207–216.
83 C. Rocchiccioli-Deltcheff, A. Aouissi, S. Launay and M. Fournier, *J. Mol. Catal. A: Chem.*, 1996, **114**, 331–342.
84 F. M. Martínez, E. Albiter, S. Alfaro, A. L. Luna, C. Colbeau-Justin, J. M. Barrera-Andrade, H. Remita and M. A. Valenzuela, *Catalysts*, 2019, **9**, 338–349.